ELSEVIER

Material modeling of the CVI-infiltrated carbon felt II. Statistical study of the microstructure, numerical analysis and experimental validation

R. Piat [a,*], I. Tsukrov [b], N. Mladenov [a], M. Guellali [c], R. Ermel [d], T. Beck [d], E. Schnack [a], M.J. Hoffmann [c]

[a] *Institute of Solid Mechanics, University of Karlsruhe, Kaiserstrasse12, D-76128 Karlsruhe, Germany*
[b] *Department of Mechanical Engineering, University of New Hampshire, Durham, NH 03824, USA*
[c] *Institute of Ceramics in Mechanical Engineering, Central Laboratory, University of Karlsruhe, Haid-und-Neu-Street 7, D-76131 Karlsruhe, Germany*
[d] *Institute of Materials Science and Engineering I, University of Karlsruhe, Kaiserstrasse12, D-76128 Karlsruhe, Germany*

Abstract

This paper employs the homogenization procedure proposed in [1] (Piat R, Tsukrov I, Mladenov N, Verijenko V, Guellali M, Schnack E, et al. Material modeling of the CVI-infiltrated carbon felt. I. Basic formulae, theory and numerical experiments. Compos Sci Technol, this issue) to predict the effective elastic properties of the CVI-densified carbon felts. It involves statistical analysis of the microstructure and approximation of pores by equivalent ellipsoids having the same volume, elongation and orientation as actual cavities.

The distribution of these ellipsoids, their orientation and volume fraction is described by a distribution function obtained from the statistical data. This function is then utilized for calculation of the effective material parameters of the composite. The procedure is validated by comparing the calculated effective properties with the results of experiments conducted on two different modifications of the infiltrated carbon felt composite.
© 2006 Elsevier Ltd. All rights reserved.

Keywords: A. Carbon–carbon composites; B. Modeling, microstructure; C. Elastic properties; E. Chemical vapour infiltration (CVI)

1. Introduction

Carbon/carbon composites manufactured using isothermal, isobaric chemical vapor infiltration (I-CVI) of carbon felts have a complex microstructure characterized by non-homogeneous distribution of irregularly shaped pores and random orientation of fibres. The pyrocarbon matrix of the composite has properties (texture) dependent on the manufacturing parameters (temperature, pressure and time length) of infiltration, see [2]. It is desirable to establish how the overall mechanical characteristics of the composite

depend on its microstructure. This paper deals with characterization and quantitative analysis of the microstructure, and investigation of dependence of the overall material properties on various microstructural parameters.

In [1], we introduced a theoretical model for prediction of the effective elastic properties of the infiltrated C-felt. The homogenisation procedure consists of two steps: (1) homogenization of material response without pores, i.e. homogenization of a media consisting of carbon fibres randomly distributed in an isotropic pyrolytic carbon matrix; (2) homogenization of material response with presence of pores, i.e. homogenization of a media consisting of three-dimensional pores embedded in the homogenized matrix from the previous step. We used the random number generator to assign the distribution of pores in the composite.

* Corresponding author. Tel.: +49 0721 608 8853; fax: +49 0721 608 4187.
E-mail address: Romana.Piat@mach.uni-karlsruhe.de (R. Piat).

The effective elastic properties were calculated as function of the fibre and pore volume fractions.

This paper analyzes the actual microstructure of several composite specimens. The pore distribution is obtained by statistical study of the polarized light microscopy images of the composite cross-sections. This information serves as input data for the numerical models developed in [1]. The calculated material parameters are then compared with the results of the tensile tests performed on the same material.

2. Microstructural analysis

The investigated I-CVI samples were embedded in a resin matrix and then polished. The microstructure of the samples was characterized by polarized light microscopy using an OLYMPUS AX70 microscope. Fig. 1 shows typical light microscopy micrographs: carbon fibres can be identified as dark ellipses or bunds, they are surrounded by gray pyrolytic carbon matrix, and then dark pores of irregular shapes. The images of the cross sections of the fibres are not circular because they are randomly oriented in the infiltrated felt, and each fibre is cut at a specific angle. Thus, the cross-sections of the fibres are presented as ellipses with the different axes.

Quantitative study shows that the composite consists of 12% (volume) of carbon fibres and the remaining 78% constitute the pyrolytic carbon matrix and pores. The open porosity of the studied material is ~5%. However, there are many closed pores, so the exact volume fraction of the pores is obtained from the statistical microstructural analysis of the cross-section images. The constituents of

the studied microstructure have the following typical dimensions: the diameter of the carbon fibres is 10 μm and the width of the pyrolytic carbon coating is 18–22 μm.

3. Pore approximation

The effective properties of the infiltrated C/C felt are computed by means of homogenization procedure which consists of two steps. In the first step, homogenization of matrix with fibres is carried out as described in [1]. For this calculation the material parameters of the pyrocarbon from [3, 4] were used. The resulting effective parameters of the homogenized material were denoted as M1 and M2, respectively. The obtained values for material with 12% volume fraction of fibres are used in this paper to predict the overall mechanical properties of porous composite.

In the second step of the homogenization, irregularly shaped pores have to be placed in the homogenized matrix with fibres. For unidirectional composites, contribution of pores can be estimated using the two-dimensional solutions for irregularly-shaped holes as described in [5,6]. Unfortunately, there are no available three-dimensional elasticity solutions for a variety of pore shapes observed in the CVI densified carbon felts. To perform micromechanical modeling, we will approximate pores by ellipsoidal shapes and utilize the well-known Eshelby solution [7,8]. Note that the accuracy of this commonly used approximation must be evaluated individually for each type of the microstructure using either experimental validation (as in the present paper) or some analytical bounding techniques (see [9] for more detail). In the case of two-dimensional irregular shapes this problem was discussed in [10]. The three-dimen-
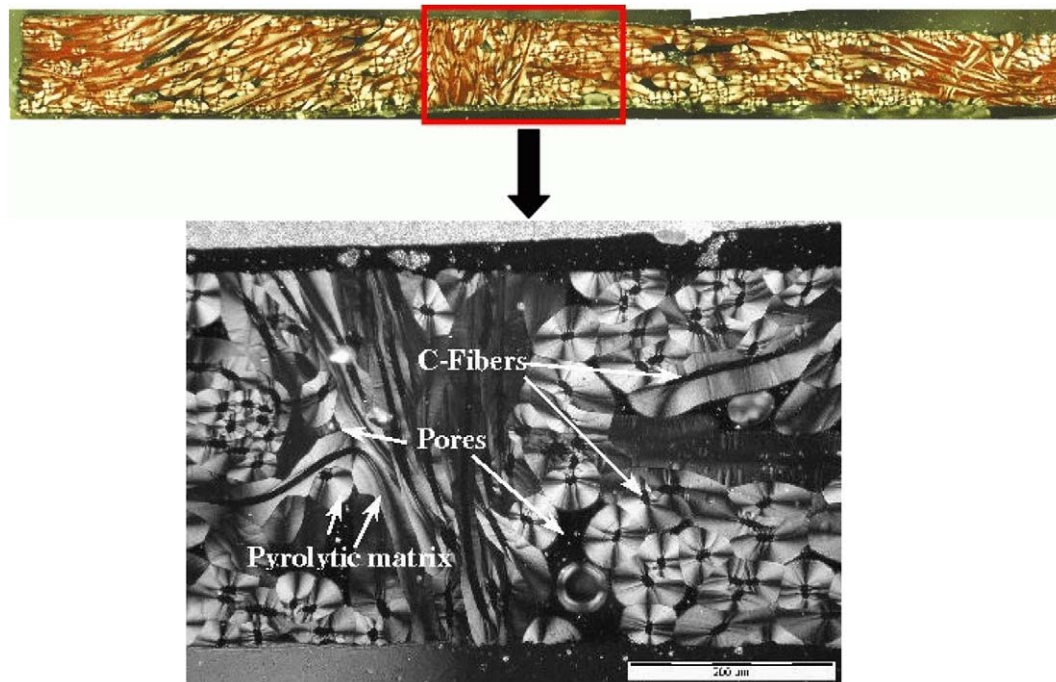

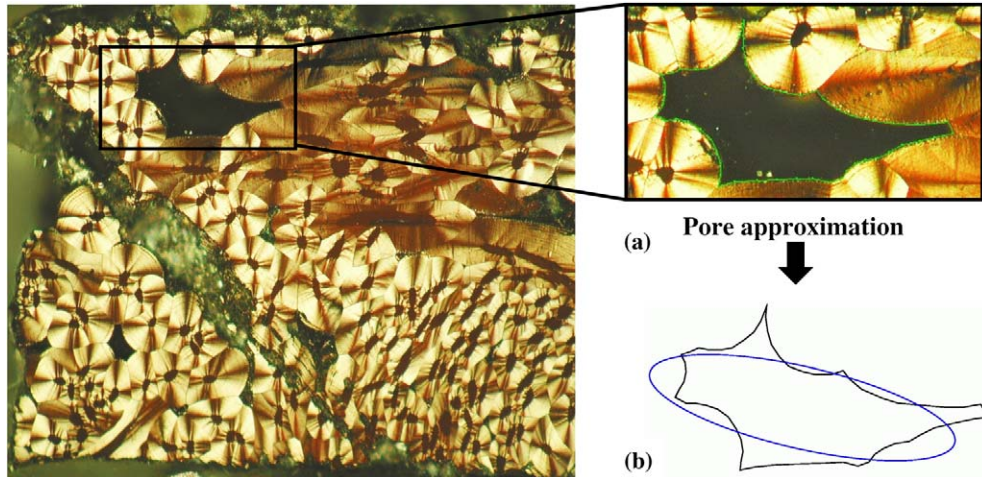Fig. 1. Cross-section of the I-CVI infiltrated carbon felt.

Fig. 2. (a) PLM micrograph of a pore on a 200 μm length scale. (b) The pore contour approximated by an ellipse.

sional approximation procedure for pores is described below.

We use two-dimensional-micrograph images, obtained by polarized light microscopy. The pore contours in the images are replaced by ellipses which are assumed to be cross-sections of the prolate or oblate three-dimensional ellipsoids. Statistical analysis of the orientation and aspect ratio of the ellipses provides distribution function for ellipsoidal pores in the composite. The inclusion compliance contribution tensor of the pores is expressed in terms of this function. Micrograph of the typical pore and approximation of the image of this pore by ellipse is presented in Fig. 2.

Each ellipse can be completely defined by three parameters: semi-axes a, b and orientation angle θ (Fig. 3). To approximate the pore contours, we assume that the largest distance between two points on the contour amounts to $2a$. Thus, the first dimension of the corresponding ellipse is known. The second dimension b satisfies

$$b = \frac{A}{\pi a}, \tag{1}$$

where A is the pore area. The orientation of the major axis $2a$ of the ellipse is chosen to coincide with the principal axis of inertia of the pore that forms smaller angle with orientation of $2a$. From two major axes of inertia of the pore presented in Fig. 3, axis 1 forms smaller angle with orientation

of $2a$ than axis 2. Hence, it becomes the axis of orientation of the corresponding ellipse. Angle θ is defined as the angle between the y-axis and the axis of orientation.

Using this procedure all pores in each cross-section can be approximated by ellipses having the same orientation, area and elongation as the actual pore. The statistical analysis of the sample cross-sections is necessary.

4. Statistical data and pore distribution function approximation

4.1. Statistical analysis of micrographs

The next step in our investigation is to obtain the data on orientational distribution and area of the pores in each direction. This is achieved by statistical analysis of several cross-sections. The number of pores and the value of porosity observed in eight studied cross-sections are given in Table 1. Using the method presented in the previous section, pores in each cross-section were approximated by ellipses, and the orientation angle, area and eccentricity parameter $\alpha = b/a$ were calculated. For three-dimensional analysis, these ellipses were assumed to be cross-sections of oblate and prolate ellipsoids.

Distribution of the values of ellipsoids' eccentricity is presented in Fig. 4. Evaluation of the total area of the
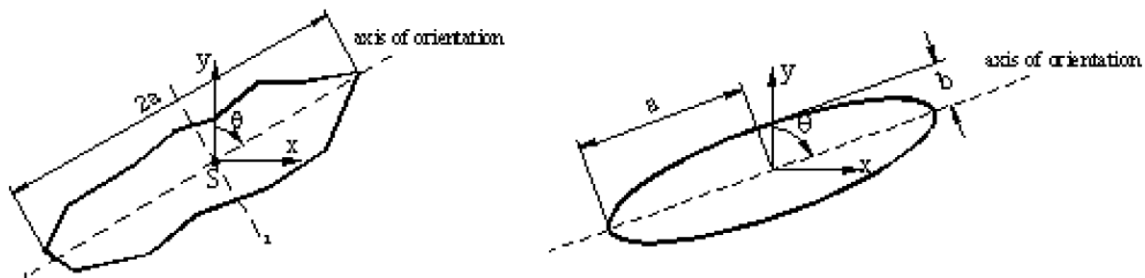

Fig. 3. (a) Schematic presentation of the contour of the pore with orientation angle θ and large axis $2a$. (b) Approximation of the same pore by ellipse with the same orientation and large axis.

Table 1
Porosity of the studied CFC cross-sections

Cross-section	Pores	Total porosity (%)
1	154	4.9
2	134	8.0
3	86	4.6
4	128	1.7
5	127	7.1
6	126	7.5
7	175	6.6
8	117	8.7

pores with eccentricities between 7 and 15 shows that these pores have very small area, and their contribution can be neglected during the subsequent calculations. Thus the bounds on eccentricity are $1.5 \leqslant \alpha \leqslant 7$ for oblate and, respectively, $0.142571 \leqslant \alpha \leqslant 0.66667$ for prolate spheroids. The statistically obtained discrete distribution of the areas of pores in each direction θ is presented in Fig. 5a. The overall total porosity obtained in these statistical studies is equal to 7.3%.

4.1.1. Pore distribution function

After the statistical investigations of cross-section micrographs of the composite, the discrete pores distribution function (Fig. 5a, line with squares) was identified and approximated by piecewise continuous Gauss-function (Fig. 5a, solid line):

$$f(\theta) = y + \frac{\sqrt{2}A_1 e^{\left(-2\frac{(\theta-x_1)^2}{\omega_1^2}\right)}}{\omega_1\sqrt{\pi}} + \frac{\sqrt{2}A_2 e^{\left(-2\frac{(\theta-x_2)^2}{\omega_2^2}\right)}}{\omega_2\sqrt{\pi}} + \frac{\sqrt{2}A_3 e^{\left(-2\frac{(\theta-x_3)^2}{\omega_3^2}\right)}}{\omega_3\sqrt{\pi}}, \tag{2}$$

where $y = 0.133352$, $x_1 = 16.0759$, $x_2 = 90.02$, $x_3 = 163.925$, $\omega_1 = 24.01$, $\omega_2 = 37.01$, $\omega_3 = \omega_1$, $A_1 = 4.16587$, $A_2 = 40.78$, $A_3 = A_1$.

Assuming the same distribution of pores in other cross-section directions, the three-dimensional distribution func-

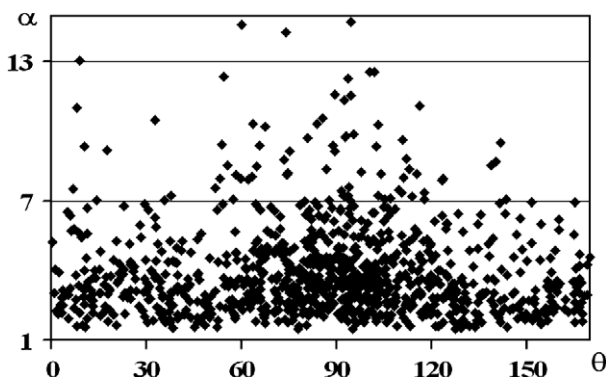Fig. 4. Eccentricity of oblate ellipsoids $\alpha = b/a$ as function of orientation angle θ.
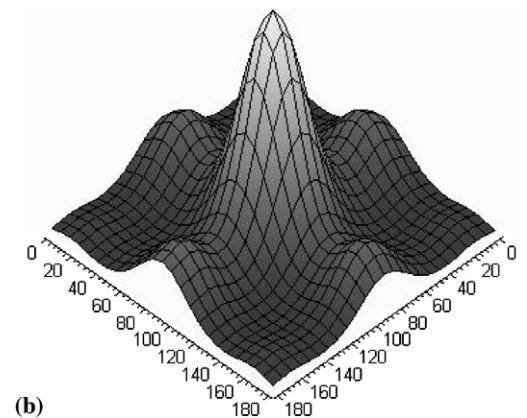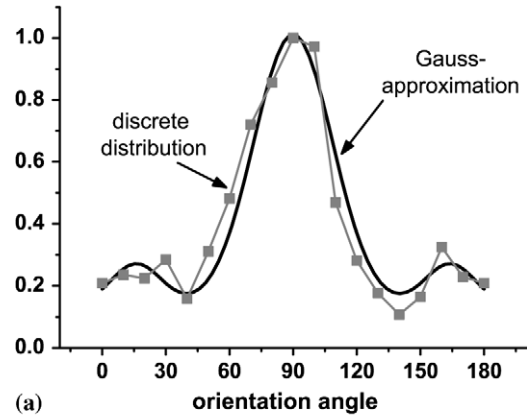

Fig. 5. Pore orientation distribution functions: (a) two-dimensional: experimental discrete and its Gauss-approximation and (b) two-dimensional: combination of two two-dimensional Gauss-approximation functions.

tion can be presented in the form $f^{3D}(\beta, \theta) = f(\beta) \cdot f(\theta)$ (Fig. 5b). This function is used to calculate the compliance contribution tensor of pores.

5. Compliance tensor of pores

In [1] we introduced the theoretical model for prediction of the effective elastic properties of infiltrated C-felt. In this model, the influence of porosity on the effective compliance of the composite was included through the overall compliance contribution tensor of the pores $\mathbf{H}^P$,

$$\mathbf{H}^P = \sum \mathbf{H}_i^{tr}, \tag{3}$$

where $\mathbf{H}_i^{tr}$ is the compliance tensor of i-Pore in the global coordinate system. If pore distribution is given by means of the continuous distribution function (2), formulae (3) can be rewritten as

$$\mathbf{H}^P = \frac{\int_{\alpha_{min}}^{\alpha_{max}} \int_{0°}^{180°} \int_{0°}^{180°} f^{3D}(\beta,\theta) \mathbf{L}^T(\beta,\theta) \mathbf{L}^T(\beta,\theta) \mathbf{H}(\alpha) \mathbf{L}(\beta,\theta) \mathbf{L}(\beta,\theta) \sin\theta \, d\theta \, d\beta \, d\alpha}{\int_{\alpha_{min}}^{\alpha_{max}} \int_{0°}^{180°} \int_{0°}^{180°} f^{3D}(\beta,\theta) \, d\theta \, d\beta \, d\alpha}, \tag{4}$$

where $\mathbf{H}(\alpha)$ is the compliance contribution tensor of a pore in the local coordinate system of the pore, $\mathbf{L}$ is the coordinate transformation matrix. The bounds on eccentricity are defined as

$$\alpha_{max} = \max \left(\frac{a}{b}\right) \quad \text{and} \quad \alpha_{min} = \min \left(\frac{a}{b}\right).$$

Their values for prolate ellipsoids are $\alpha_{min} = 1.5$ and $\alpha_{max} = 7$; for oblate ellipsoids, $\alpha_{min} = 0.142571$ and $\alpha_{max} = 0.66667$. After calculation of the compliance tensor of pores, the effective compliance of the composite can be found as $\mathbf{D}^{eff} = \mathbf{D}^{MT} + \mathbf{H}^P$, where $\mathbf{D}^{MT}$ is the overall compliance of the material consisting of the pyrocarbon matrix and fibres, calculated using the Mori-Tanaka micromechanical method as presented in [1].

6. Numerical analysis

The effective elastic properties of two composites (with different elastic properties of pyrocarbon matrix) were calculated. Results obtained for material with pyrocarbon matrix having Young's modulus $E_{M1} = 25.0$ GPa and Poisson's ratio $v_{M1} = 0.15785$ (given by Kostka et al. [3]) are denoted by subscript M1; results for material with $E_{M2} = 38.556$ GPa and $v_{M2} = 0.16$ (given by Papadakis and Bernstein [4]) are presented with subscript M2. In both simulations the mechanical properties of carbon felt were assumed to be $E_f = 200$ GPa, $v_f = 0.27$. The effective Young's moduli, $E^{eff}_{M1+porosity}$ and $E^{eff}_{M2+porosity}$, Poisson's ratios $v^{eff}_{M1+porosity}$ and $v^{eff}_{M2+porosity}$, and shear moduli,

$\mu^{eff}_{M1+porosity}$ and $\mu^{eff}_{M2+porosity}$, were obtained using the pore distribution function $f^{3D}(\beta, \theta)$ found in Section 4. The difference between $v^{eff}_{M1+porosity}$ and $v^{eff}_{M2+porosity}$ is practically very small, so we present only one graph for this material parameter.

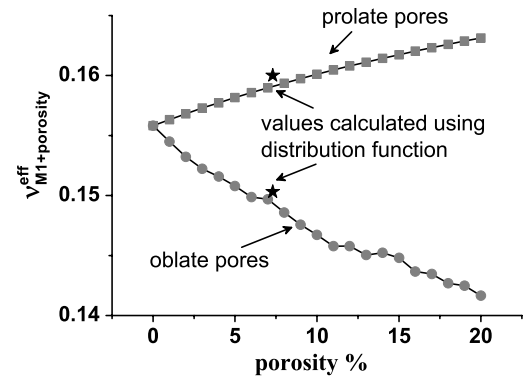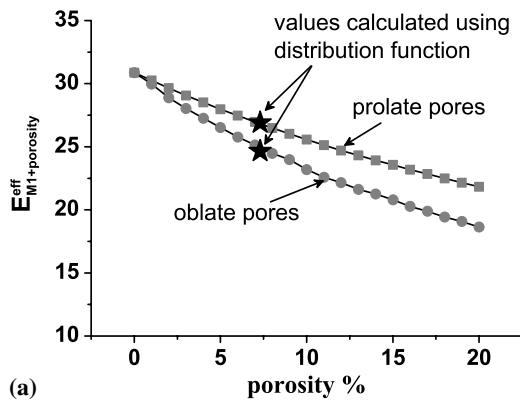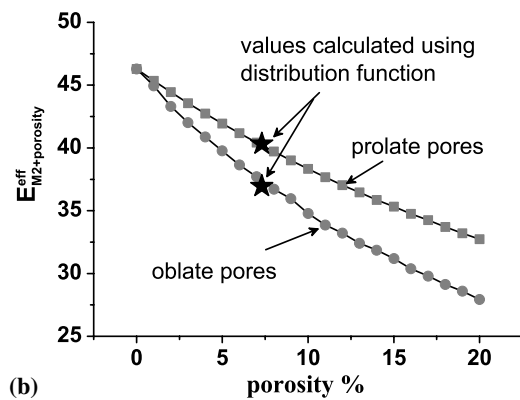Figs. 6–8 provide values of the effective engineering constants as functions of porosity.

Fig. 7. Poisson ratio of material M1 with randomly distributed pores characterized by the distribution function $f^{3D}(\beta, \theta)$ compared to results obtained using random numbers generator for distribution of oblate and prolate spheroids.

(a)
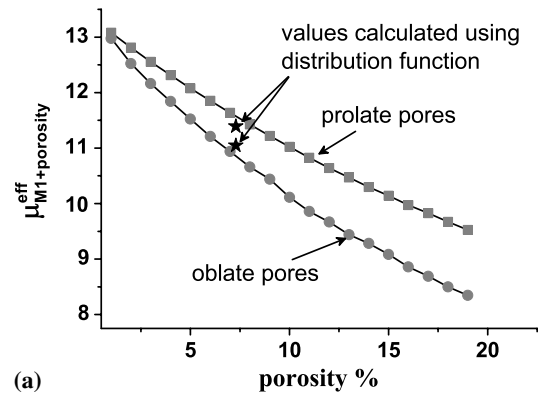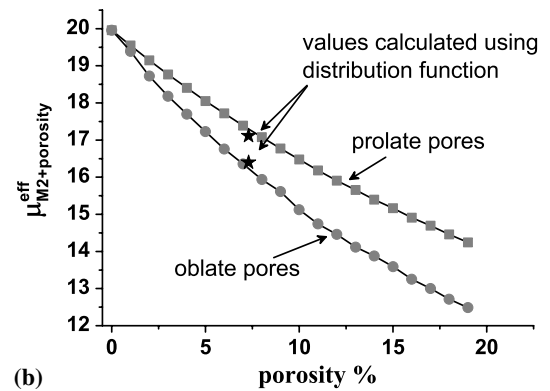
(b)

Fig. 6. Young's modulus of M1 and M2 materials with randomly distributed pores characterized by the distribution function $f^{3D}(\beta, \theta)$ compared to the results obtained using random numbers generator for pore distribution of oblate and prolate spheroids.

(a)

(b)

Fig. 8. Shear modulus of M1 and M2 materials with different properties of the pyrocarbon matrix (M1 and M2) with randomly distributed pores characterized by the distribution function $f^{3D}(\beta, \theta)$ compared to the results obtained using random numbers generator for distribution of oblate and prolate spheroids.

Table 2
Effective elastic properties calculated using pore distribution function (2)

Parameter	CFC 1 (M1)		CFC 2 (M2)	
	Oblate	Prolate	Oblate	Prolate
E_1^{eff} (GPa)	26.0969	26.1656	39.1232	39.2250
E_2^{eff} (GPa)	26.9016	24.6453	40.3284	36.9465
E_3^{eff} (GPa)	25.9184	26.5419	38.8558	39.7887
ν_{12}^{eff}	0.1584	0.1515	0.1618	0.1546
ν_{32}^{eff}	0.1608	0.1503	0.1642	0.1534
ν_{13}^{eff}	0.1664	0.1541	0.1696	0.1574
μ_{12}^{eff} (GPa)	11.4497	10.9692	17.1141	16.3982
μ_{32}^{eff} (GPa)	11.3926	11.0477	17.0294	16.5151
μ_{13}^{eff} (GPa)	11.1499	11.4016	16.6693	17.0423

Each graph presents the following results: effective values calculated using the random number generator for oblate (line with squares) and prolate (line with circles) spheroidal pores (as described in [1]), and the corresponding values calculated for randomly distributed oblate and prolate pores using the experimentally obtained pore orientations distribution function $f^{3D}(\beta, \theta)$.

Table 2 presents the numeric values of the effective elastic properties for materials M1 and M2 calculated using the distribution function $f^{3D}(\beta, \theta)$.

7. Experimental results and modeling validation

Verification of the obtained theoretical results was conducted by comparing numerical predictions for Young's modulus with the experimentally obtained values. Two CVI-densified C-fibre felts with different pyrocarbon matrix but similar volume fraction, orientation of the fibres and pores, and the same width of the pyrolytic carbon coating on the fibres were available. The difference in pyrocarbon matrix was characterized by the level of texture: felt 1 exhibited a high-textured matrix, while in the case of felt 2 the matrix was low-textured [11–14]. The tests were performed on the electromechanical testing machine with a constant crosshead velocity of 0.1 mm/min. The strain was measured by the optical extensometer which allows an integral as well as a locally resolved determination of the strains. The geometry and dimensions of the tensile specimens are shown in Fig. 9.

The results of mechanical testing are summarized in Table 3 for 17 samples of each type. Two typical stress–strain curves are presented in Fig. 10.

The mean value of Young's modulus for felt 2 is $E_{\text{F2}} = 21.6$ GPa as compared to $E_{\text{F1}} = 18.6$ GPa of felt 1. Furthermore, a pronounced higher total strain at failure ε_t of felt 1 can be recognized whereas the difference in strength between two types of materials is small.
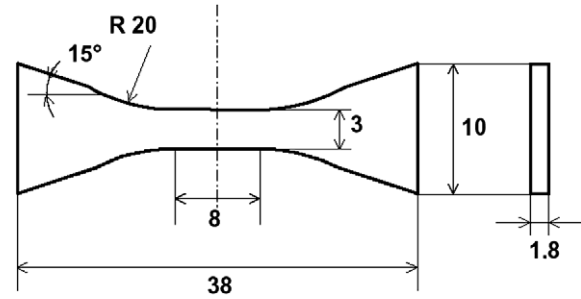

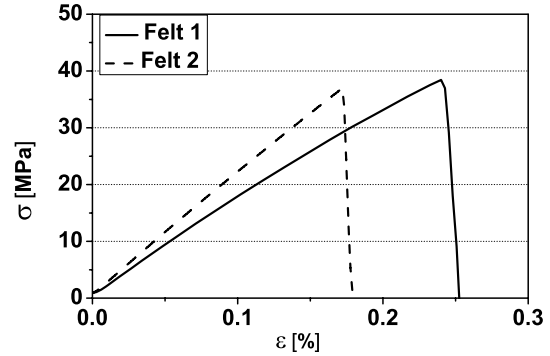Fig. 9. Geometry of tensile specimen (dimensions in mm).

Fig. 10. Results of tensile tests for two materials with different pyrolytic carbon matrix (felt 1 and felt 2).

The results of mechanical testing with $18.6 \pm 1.0 \leqslant E \leqslant 21.6 \pm 1.9$ are sufficiently close to the calculated value for material M1.

8. Conclusions

In this paper, the theoretical approach proposed in [1] was used for calculation of the effective elastic moduli for actual material microstructures. Firstly, statistical studies of the cross-sectional micrographs of material were carried out. During these investigations the pores with irregular shapes were approximated as ellipsoids. The volume fraction, eccentricities and orientation of the ellipsoids were chosen based on the information on actual pores in the material. The three-dimensional pore distribution function was constructed, and the theoretical solution presented in [1] was rewritten for this case.

The overall compliance tensor of the material with experimentally obtained pore distribution function was calculated and these results were compared with the results obtained using the random numbers generator for the same porosity. Both results are close to each other.

The results of tensile test for the material having the same microstructure as the statistically investigated one

Table 3
Results of mechanical testing and material characterization (mean values and standard deviation)

Material	Number of specimens	Open porosity (%)	$\sigma_{\max}$ (MPa)	E (GPa)	ε_t (%)
Felt 1	17	4.6 (3.1–6.2)	38.4 ± 6.6	18.6 ± 1.0	0.23 ± 0.04
Felt 2	17	5.3 (4.7–5.9)	35.0 ± 9.1	21.6 ± 1.9	0.18 ± 0.05

were compared with theoretical predictions. The values of the Young's modulus obtained experimentally are close to the results predicted using the pores distribution function for material M1.

Acknowledgements

References

[1] Piat R, Mladenov N, Tsukrov I, Verijenko V, Guellali M, Schnack E, et al. Material modeling of the CVI-infiltrated carbon felt. I. Basic formulae, theory and numerical experiments. Compos Sci Technol this issue, doi:10.1016/j.compscitech.2006.02.008.

[2] Guellali M, Oberacker R, Hoffmann MJ. Influence of the matrix microstructure on the mechanical properties of CVI-infiltrated carbon fiber felts. Carbon 2005;43(9):1954–60.

[3] Kostka H, Birkle S, Küsebauch W. Pyrokohlenstoff-Eigenschaften und Anwendung. Mat-wiss U Werkstofftech 1989;20:92–100.

[4] Papadakis EP, Bernstein H. Elastic moduli of pyrolytic graphite. J Acoust Soc Am 1963;35(4):521–4.

[5] Tsukrov I, Novak J. Effective elastic properties of solids with defects of irregular shapes. Int J Solids Struct 2002;39:1539–55.

[6] Tsukrov I, Piat R, Novak J, Schnack E. Micromechanical modeling of porous carbon/carbon composites. Mech Adv Mater Struct 2005;12(1):43–54.

[7] Eshelby JD. The determination of the elastic field of an ellipsoidal inclusion, and related problems. Proc Roy Soc A 1957;241:376–96.

[8] Mura T. Micromechanics of defects in solids. second ed. Dordrecht: Kluwer; 1987.

[9] Kachanov M, Sevostianov I. On quantitative characterization of microstructures and effective properties. Int J of Solids Struct 2005;42(2):309–36.

[10] Tsukrov I, Kachanov M. Solids with holes of irregular shapes: effective moduli and anisotropy. Int J Fract 1993;64:R9–R12.

[11] Reznik B, Hüttinger KJ. On the terminology for pyrolytic carbon. Carbon 2002;40(4):621–4.

[12] Piat R, Reznik B, Schnack E, Gerthsen D. Modeling the effect of microstructure on the elastic properties of pyrolytic carbon. Carbon 2003;41(9):1858–61.

[13] Reznik B, Gerthsen D, Zhang W, Hüttinger KJ. Texture changes in the matrix of an infiltrated carbon fiber felt studied by polarized light microscopy and selected area electron diffraction. Carbon 2003;41(2):376–80.

[14] Guellali M. Einfluss der Abscheide- und Heißpressbedingungen auf die Mikrostruktur und Eigenschaften von CVI-CFC-Werkstoffen. Schriftenreihe des Instituts für Keramik im Maschinenbau, IKM 040. Universität Karlsruhe (TH), PhD Thesis; 2003.